9-2012

Prospects for nanoparticle-based permanent magnets

Balamurugan Balamurugan
University of Nebraska-Lincoln, balamurugan@unl.edu

David J. Sellmyer
University of Nebraska-Lincoln, dsellmyer@unl.edu

George C. Hadjipanayis
University of Delaware, hadji@udel.edu

Ralph Skomski
University of Nebraska-Lincoln, rskomski2@unl.edu

Published in *Scripta Materialia* 67:6 (September 2012), pp. 542–547; doi: 10.1016/j.scriptamat.2012.03.034

Published online April 4, 2012.

Prospects for nanoparticle-based permanent magnets

B. Balamurugan,[a, b] D. J. Sellmyer,[a, b] G. C. Hadjipanayis,[c] and R. Skomski[a, b]

a. Nebraska Center for Materials and Nanoscience, University of Nebraska–Lincoln, Lincoln, NE 68588, USA
b. Department of Physics and Astronomy, University of Nebraska–Lincoln, Lincoln, NE 68588, USA
c. Department of Physics and Astronomy, University of Delaware, Newark, DE 19716, USA

Corresponding author — D. J. Sellmyer, Department of Physics and Astronomy, University of Nebraska–Lincoln, Lincoln, NE 68588, USA; email dsellmyer@unl.edu

Abstract
Magnetic nanoparticles smaller than ~15 nm in diameter and with high magnetocrystalline anisotropies $K_1 \geq 1$ MJ m^{-3} can be used as building blocks for next-generation permanent magnets. Advances in processing steps are discussed, such as self-assembly, alignment of the easy axes and appropriate nanostructuring that will enable the fabrication of densely packed nanoparticle assemblies with improved permanent-magnet properties. This study also proposes an idealized nanocomposite structure for nanoparticle-based future permanent magnets with enhanced energy products.

Keywords: nanoparticle building blocks, exchange-coupled nanocomposites, permanent-magnets, synthesis, processing

1. Introduction and scope

Permanent magnets are used in a wide range of applications from energy-conversion devices (motors, loudspeakers, and electric generators and alternators), household appliances and cell phones to recent environmentally friendly technologies such as hybrid vehicles and wind turbines [1–4]. This increasing demand has led to impressive progress in permanent magnets for most of the 20th century through discovery of new materials and improvement in their energy products $(BH)_{max}$ [2–4]. $(BH)_{max}$ strongly depends on the saturation magnetic polarization ($J_s = 4\pi M_s$ or $\mu_0 M_s$, where M_s is the saturation magnetization) and coercivity (H_c), which originates from the magnetic anisotropy (K_1) and ferromagnetic ordering in these materials [5, 6]. The rare-earth-based magnets, especially $SmCo_5$ (K_1 = 17 MJ m^{-3} and J_s = 10.7 kG or 1.07 T) and $Nd_2Fe_{14}B$ (K_1 = 5 MJ m^{-3} and J_s = 16.1 kG) are stronger magnets so far, owing to their high K_1 and J_s at room temperature [7, 8] and thus have an ever-increasing demand, but further improvement in their performance has been slowing in recent years [2–4]. $L1_0$-ordered (face-centered tetragonal) FePt alloys have shown superior permanent-magnet properties with K_1 = 7 MJ m^{-3} and J_s = 13.8 kG among the rare-earth-free alloys, but the high cost of Pt is a limiting factor.

Next-generation permanent magnets can be fabricated using nanoparticles with size below ~15 nm as building blocks to improve some of their properties by exploiting nanoscale effects, and also to miniaturize the devices to suit the modern technological requirements [9–12]. A typical example is the development of exchange-coupled nanocomposites made of a fine mixture of magnetically hard and soft nanoparticles with well-controlled compositions and interfaces [10, 11]. In this way, the cost of the rare-earth or $L1_0$-ordered FePt-based magnets can be lowered, and the prospects for high-anisotropy materials ($K_1 \geq 1$ MJ m^{-3}) with moderate J_s (≤ 10 kG) can also be increased for permanent-magnet applications by combining them with materials such as $Fe_{65}Co_{35}$ with a high J_s of ~24 kG.

There are, however, several formidable tasks ahead to implement nanoparticle building blocks as permanent magnets. First, synthesis of magnetic nanoparticles with precise control over the size, size distribution and phase purity is challenging, owing to the requirement of high-temperature thermal annealing >500 °C under thermal-equilibrium conditions [13–15]. Second, the particles must be assembled with their easy axes aligned to obtain a large remanent magnetization (M_r). Note that M_r/M_s is only ~0.5 for isotropic samples [5, 6, 16], which can be enhanced significantly only by aligning their easy axes. In addition, compaction of magnetic nanoparticles is important to de-

velop permanent magnets with high-packing densities and M_r close to M_s. This paper presents an overview of recent research developments on magnetic nanoparticles and emphasizes various processing steps to improve their prospects for future permanent-magnet applications using rare-earth cobalt (R-Co) alloys, especially RCo_5 (R = Y, Sm) and FePt as typical examples.

2. Nanoparticle synthesis, structure and self-assembly

The synthesis of permanent-magnet nanoparticles should provide excellent control of the size, size distribution, self-assembly and crystalline ordering. In particular, the desired crystalline ordering in permanent-magnet nanoparticles, e.g., the hexagonal $CaCu_5$-type in RCo_5 alloys and face-centered tetragonal structure ($L1_0$-chemical ordering) in FePt, is important to obtain the high anisotropies in these materials to realize their permanent-magnet properties [17–19].

2.1. Chemical methods

Wet-chemical techniques are suitable for producing monodisperse and self-assembled nanoparticles of average sizes tunable from 3 to 15 nm, which are generally produced by the reduction or decomposition of metal salts in the presence of stabilizing or capping agents [9, 10, 20–23]. For example, the reduction of platinum acetylacetonate and decomposition of iron pentacarbonyl in the presence of oleic acid and oleylamine stabilizers results in monodisperse FePt nanoparticles [9], which can be deposited as self-assembled nanoparticle arrays on suitable substrates using spin or dip-coating. The stabilizing molecules attached to the growing nanoparticles control the particle size and size distribution during synthesis, and also result in the formation of self-assembled structures on substrates, as shown in the transmission electron microscopy (TEM) image of FePt nanoparticles (Figure 1). The as-produced FePt nanoparticles, however, have the disordered face centered cubic (fcc) structure, and subsequent thermal annealing >500 °C under inert-gas atmosphere is required to form the $L1_0$-ordering [9]. In addition, wet chemical techniques have shown limited success in the synthesis of rare-earth alloy nanoparticles with a high degree of crystalline ordering and phase purity [24, 25].

2.2. Physical methods: cluster deposition

The cluster-deposition method using physical vapor deposition processes such as sputtering, thermal evaporation or laser ablation is based on the inert-gas-condensation principle and has been successful in producing both FePt and rare-earth alloy nanoparticles of smaller sizes (2–15 nm) with uniform size distribution and a high degree of atomic ordering [18, 26–32]. For example, the sputtering of atoms from the solid surface of a desired composition (such as YCo_5 or FePt) in a cooled inert-gas atmosphere (mixture of Ar and He)>10^{-2} torr leads to successive collisions of sputtered atoms with the inert gas ions, and thus results in the formation of nanoparticles in the gas phase prior to deposition on substrates kept at room temperature [18, 27, 30, 32]. This method produces monodisperse nanoparticles of size $d \leq 10$ nm with an rms standard deviation $\sigma/d \approx 0.15$, as shown in the TEM image of YCo_5 nanoparticles (Figure 2) and corresponding particle size histogram (top inset of Figure 2) [18].

Compared with chemical methods, the desired crystalline ordering in the case of rare-earth alloy [18, 27] and FePt nanoparticles [30] can be obtained directly without subsequent heat treatment using high sputtering powers (≤ 120 W) or modifying the plasma conditions as revealed in the high-resolution TEM (HRTEM) image of the directly ordered YCo_5 nanoparticles (bottom inset of Figure 2). Assembly of cluster-deposited nanoparticles, for example FePt, has been achieved by depositing them onto Si substrates, which are pre-coated with multilayers of amphiphilic phospholipid molecules [33, 34].

2.3. Surfactant-assisted ball milling

Bulk permanent-magnet alloys are traditionally obtained by conventional arc-melting, followed by a high-temperature homogenization heat treatment, which results in grains of size >100 μm [13, 14]. The conventional ball-milling process, in which bulk alloys are ground to fine powders using a grinding medium such as ceramic or stainless-steel balls, reduces the grain size only to ~30 nm [13, 14]. The ball milling of rare-earth alloys such as Nd–Fe–B or Sm–Co in a liquid medium (heptane) as well as in the presence of stabilizing agents such as oleic acid or oleylamine, however, can reduce the particle size to 5 nm [35–39]. Interestingly, these nanoparticles deposited on substrates such as carbon-coated Cu grids also show self-assembly, presumably caused by the presence of the surfactants [38].

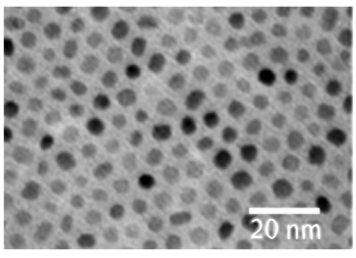

Figure 1. TEM image showing the self-assembly of FePt nanoparticles produced by the chemical method. (Reprinted with permission from Reference [23], copyright 2007 American Chemical Society.)

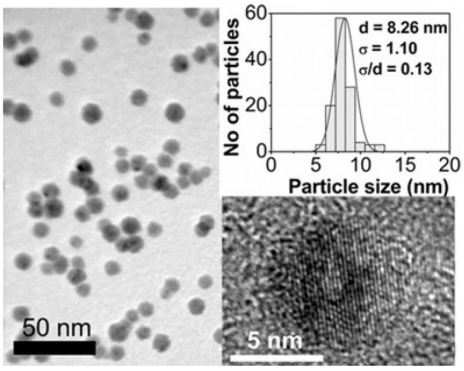

Figure 2. TEM image of cluster-deposited YCo_5 nanoparticles, where particle-size histogram (top) and high-resolution TEM image of a single nanoparticle showing lattice fringes (bottom) are given as insets. (Reprinted with permission from Reference [18], copyright 2011 American Chemical Society.)

3. Magnetic properties of nanoparticles

Size effects, especially the presence of superparamagnetism and the surface modification by oxidation or surfactant molecules are critical factors affecting H_c and J_s of nanoparticles [3, 24, 25, 40]. RCo_5 (Y, Sm) and $L1_0$-FePt alloys retain their ferromagnetic ordering for nanoparticle sizes down to ~3 nm as well as their high K_1[8]. RCo_5 nanoparticles are, however, sensitive to surface oxidation, which reduces H_c and J_s[25]. Cluster-deposition methods performed under high-vacuum conditions usually prevent the surface oxidation of rare-earth elements. These particles can exhibit appreciable H_c values (2–8 kOe) at room temperature and a high J_s (~10 kG), comparable with their bulk values, as shown in the magnetization (M) vs applied field (H) loops (Figure 3a) [18, 27, 41]. Similarly, $SmCo_5$ and $Nd_2Fe_{14}B$ nanoparticles of diameter ~10 nm produced by surfactant-assisted ball milling exhibit high H_c at room temperature in the range ~2.0–18.6 kOe and 1.2–4.0 kOe, respectively [37, 38]. $L1_0$-FePt nanoparticles have superior chemical stability and show high H_c up to 20 kOe at room temperature for nanoparticles with sizes varying from 4 to 10 nm produced by both the cluster-deposition and wet-chemical techniques [9, 22, 29, 30].

Both RCo_5 and FePt nanoparticles have shown high K_1 values comparable with their bulk values. It is worth noting that these nanoparticles are often exchange-coupled to each other, which leads to a reduction in H_c through the magnetic reversal by the propagation of interaction-domain walls. However, H_c can be further improved by producing exchange-decoupled nanoparticles, which are expected to show Stoner–Wohlfarth-type behavior with H_c scaling directly with their magnetic anisotropies according to $2K_1/M_s$ [5, 6, 16, 22, 29]. For example, cluster-deposited FePt nanoparticles dispersed in a non-magnetic carbon matrix exhibited a high H_c = 29 kOe at room temperature, as shown in Figure 3b, and H_c increases further to 40 kOe at 4.2 K [29, 32]. The easy axes of these nanoparticles are generally distributed randomly, as revealed by the identical in-plane and out-of-plane hysteresis loops measured in the case of FePt nanoparticles (Figure 3b) and this leads to $M_r/M_s \approx 0.5$.

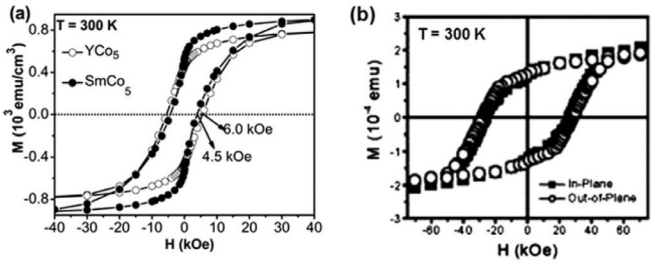

Figure 3. Hysteresis loops measured at 300 K for cluster-deposited permanent-magnetic nanoparticles: (a) in-plane hysteresis loops of directly ordered YCo_5 (reprinted with permission from Reference [18], copyright 2011 American Chemical Society) and $SmCo_5$ [27, 41]; (b) in-plane and out-of-plane hysteresis loops of dilute-FePt nanoparticles (5% in volume) dispersed in SiO_2 matrix [29, 32] (reprinted with permission from Reference [29], copyright 2005 American Institute of Physics).

4. Processing including alignment

The Stoner–Wohlfarth model predicts M_r/M_s = 0.5 for a random distribution of non-interacting uniaxial single-domain particles; a deviation from this ideal value is, however, observed in real systems, owing to interparticle interactions and textured growth [5, 6, 16]. RCo_5 and $L1_0$-FePt nanoparticles prepared by both wet-chemical and cluster-deposition methods are typically found to have $M_r/M_s \approx 0.5$ [9, 18, 22, 29, 30], and this is one of the limiting factors affecting $(BH)_{max}$ for nanoparticle-based permanent magnets. M_r/M_s can be increased to some extent in the case of exchange-coupled nanocomposites [10]. A significant increase in M_r/M_s is only possible by aligning the easy axes of nanoparticles in a particular direction (either in-plane or perpendicular) during growth or deposition process. A complete alignment of the easy axes of Stoner–Wohlfarth particles should ideally result in a rectangular hysteresis loop with M_r/M_s = 1 along the easy-axis direction and a hysteresis loop with $M_r/M_s \approx 0$ along the hard axis, which saturates or joins the easy-axis loop at M corresponding to the anisotropy field (H_a), as shown in Figure 4a. In the case of interacting nanoparticles, H_c is also expected to increase with the easy-axis alignment.

The cluster-deposition method is capable of producing directly ordered permanent-magnet nanoparticles by aligning their easy axes through applications of a magnetic field using a set of permanent magnets prior to deposition on substrates [18, 30, 31, 41–43]. The alignment process causes a significant increase in H_c and M_r/M_s in the easy-axis direction compared with those in the hard-axis direction as shown in the case of magnetically aligned $SmCo_5$ nanoparticles (Figure 4b) [41]. However, chemical methods require high-temperature annealing to obtain the desired crystalline ordering. Annealing of self-assembled fcc FePt nanoparticles in a very large magnetic field to produce simultaneously the $L1_0$-ordering and easy-axis alignment was unsuccessful, presumably because the temperature required for a higher ordering is above their Curie temperature [44, 45]. The surfactant-assisted chemical method performed at a moderate temperature of ~350 °C and subsequent alignment using a magnetic field of 20 kOe could obtain only partially ordered and aligned $L1_0$-FePt nanoparticles [46]. In comparison, the ball-milling process showed preferential texturing in some cases, which makes them magnetically anisotropic [37]. This can be improved further by alignment of their easy axes using a magnetic field as clearly seen in the M–H loops of magnetically

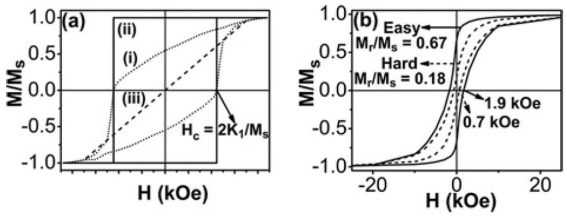

Figure 4. (a) Ideal hysteresis loops for exchange-decoupled systems: (i) randomly oriented nanoparticles, (ii) easy-axis and (iii) hard axis loops for magnetically aligned nanoparticles. (b) Hysteresis loops of magnetically aligned $SmCo_5$ nanoparticles using a field of 5 kOe measured at 300 K in the easy axis and hard axis directions [41].

aligned $SmCo_5$ nanoparticles measured in the in-plane and out-of-plane directions (Figure 5) [38].

5. Magnetic properties of nanoparticle composites

When a magnetically hard material with a high H_c (curve i in Figure 6) and a thin soft material with a low H_c and a large J_s (curve ii in Figure 6) are combined, magnetic moments in both layers are expected to switch coherently, and the resultant H_c and J_s will be some average from the constituent phases (curve iii in Figure 6). This concept of exchange coupling brought a new hope for the improvement of $(BH)_{max}$ of permanent magnets [47–53]. For an efficient exchange coupling, the characteristic dimension of the soft phase cannot exceed about twice the wall thickness of magnetic domains in the hard phase, which typically limits the size of the soft grains to ~10 nm, and the volume fraction of the soft phase must not be too high in order to lose a large H_c value, which limits the $(BH)_{max}$ of the composite [50–52].

Nanocomposite magnets have been prepared using wet-chemical [10, 17], cluster-deposition and ball-milling methods [47–49, 54, 55]. For example, a TEM image of self-assembled FePt–Fe_3Pt nanocomposites prepared by a simple mixing of FePt and Fe_2O_3 nanoparticles and subsequent thermal annealing is shown in Figure 7a [10, 17]. Their magnetic properties, such as H_c and J_s, are tailored as a function of Fe_3O_4:FePt mass ratios, as illustrated in Figure 7b [10, 17]. However, as indicated in Figure 7b, a maximum of $(BH)_{max}$ of ~20.1 MGOe was observed only for a small fraction of soft phase (Fe_3O_4:FePt mass ratio of 0.1), compared with 14.7 MGOe of the pure $L1_0$-ordered FePt nanoparticles. Similarly, $Sm(Co_{0.80}Fe_{0.20})_5$:$Fe_{65}Co_{35}$ and $Sm_2(Co_{0.82}Fe_{0.18})_7$:$Fe_{65}Co_{35}$ fabricated using the ball-milling process followed by high-pressure compaction and subsequent high-temperature thermal annealing shows a $(BH)_{max}$ of 19.2 MGOe for 25 wt.% of $Fe_{65}Co_{35}$ [47, 48]. An increase in $(BH)_{max}$ is not possible in these types of nanocomposites for a large inclusion of soft phase, owing to a substantial reduction in H_c caused by domain-wall pinning.

An increasing energy product with a large inclusion of soft phase up to ~50 vol.% was, however, possible in the case of exchange decoupled composite nanoparticles composed of $L1_0$-FePt and fcc Fe_3Pt phase. For example, $L1_0$-FePt:fcc Fe_3Pt nanocomposite particles separated by SiO_2 or C matrix layers were produced by the cluster-deposition method, and the estimated $(BH)_{max}$ curves from both the experimental and micromagnetic simulations show a maximum of ~25 MGOe for ~50 vol.% of soft Fe_3Pt phase, as shown in Figure 8 [55]. The high-energy product is possible in part because the composite particles have large soft-phase content and are reasonably isolated, so that magnetic reversal by the propagation of domain walls is not possible [54, 55]. Although this isotropic model structure neglects the inter-particle non-magnetic regions, the future development of permanent magnets may be accomplished by increasing the magnetic nanoparticle volume fraction, but maintaining a decoupling between the particles by developing, for example, a thin non-magnetic shell structure as shown in Figure 9.

6. Idealized nanocomposite structure

Based on the above-mentioned observations, various schemes for exchange-coupled nanocomposite structures composed of hard and soft phases are illustrated in Figure 9.

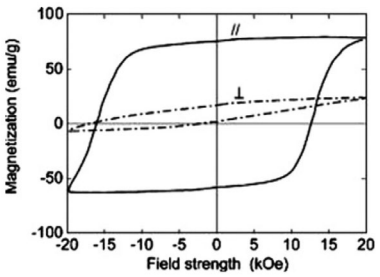

Figure 5. Room-temperature hysteresis loops of aligned $SmCo_5$ nanoparticles produced by surfactant-assisted ball milling measured in the in-plane and out-of-plane directions. (Reprinted with permission from Reference [38], copyright 2009 American Institute of Physics.)

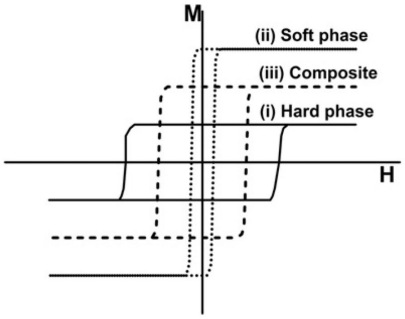

Figure 6. Typical hysteresis loops: (i) a hard phase, (ii) a soft phase and (iii) the exchange-coupled nanocomposites made of the soft and hard phases.

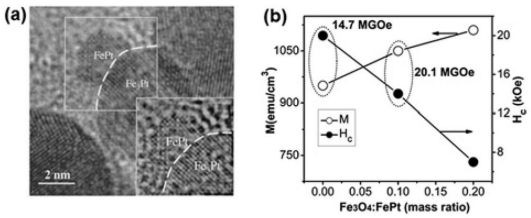

Figure 7. (a) TEM image (reprinted with permission from Reference [17], copyright 2003 American Institute of Physics), and magnetic properties of FePt–Fe_3Pt nanocomposites fabricated by wet-chemical method [10, 17].

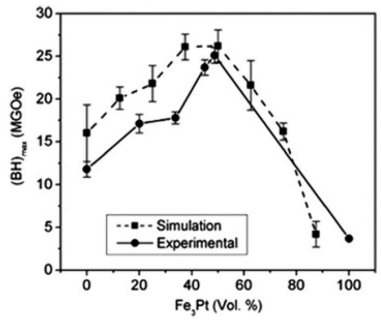

Figure 8. Magnetic properties of exchange-decoupled FePt–Fe_3Pt nanocomposites fabricated by cluster-deposition method. (Reprinted with permission from Reference [55], copyright 2008 Elsevier.)

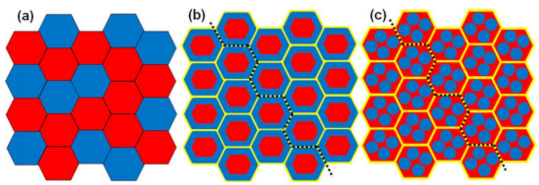

Figure 9. Various schemes for the exchange-coupled nanocomposite structures composed of magnetically hard (red) and soft (blue) nanoparticles: (a) conventional structure with soft and hard nanoparticles; (b) core–shell hard–soft nanoparticles and (c) nanocomposite particles with a non-magnetic layer (yellow), where the pinning of domain walls is indicated by black-dotted lines.

For an ideal exchange-coupling, the magnetic reversal of the hard and soft phases must occur simultaneously in nanocomposites. The nanocomposite structure as illustrated in Figure 9a is similar to the chemically prepared FePt–F_3Pt and compacted $SmCo_5$:$Fe_{65}Co_{35}$ nanocomposites discussed earlier [10, 47, 48, 17]. If the dimension of the soft phase is too large, magnetic reversal initiates in the soft magnetic phase, owing to its lower anisotropy. This process leads to the propagation of domain walls and results in a reduction in coercivity and remanent magnetization at a large fraction of soft phases. Thus, developing a nanostructure as schematically shown in Figure 9b and c, which inhibits domain expansion by pinning of domain walls using a non-magnetic layer around the nanocomposite particles, would significantly improve the magnetic properties by maintaining coercivity at high soft magnetic-phase fractions. This is also evident from the cluster-deposited FePt–Fe_3Pt nanocomposite particles dispersed in SiO_2 matrix [54, 55].

Fe–Pt and Sm–Co-based nanocomposites reported so far are isotropic magnets [10, 47, 48] and the $(BH)_{max}$ of ~25 MGOe observed in these composites is less than that of anisotropic $Nd_2Fe_{14}B$-based magnets (64 MGOe). Thus, If the easy axis of the hard phases in the nanocomposite particles in Figure 9b and c is aligned in one direction, $(BH)_{max}$ is expected to be enhanced, owing to the improved M_r/M_s and H_c upon alignment. A nanocomposite structure similar to that in Figure 9c, in which the easy axis of the hard phase is aligned, has been produced recently in FePt:Fe_3Pt thin film systems [56], and these nanocomposites show an impressive energy product of ~54 MGOe. This type of nanostructure must be fabricated at the nanoscale using both chemical and cluster-deposition methods. For example, directly ordered nanocomposites particles can be produced using the cluster-deposition process and subsequently be aligned with the easy axis of hard phase and coated with a thin non-magnetic layer, prior to deposition. The formation of a thin layer of non-magnetic material is possible by employing a sputtering or evaporation source between the cluster-formation and deposition chambers [57–59]. While the thin non-magnetic layer eliminates the inter-composite particle interactions and can enhance the amount of inclusion of soft phases compared with the hard phase without much reduction in coercivities, the magnetic alignment is expected produce an ideal square loop with $M_r/M_s = 1$. However, the scale-up of the cluster-deposition method for large-scale production has not yet been considered. In addition, nanocomposites can be produced on a large scale using chemical and surfactant-assisted ball-milling processes and compacted under high pressure, but here the easy-axis alignment is a problem that needs to be solved.

7. Concluding remarks

Synthesis, self-assembly and easy-axis alignment of monodisperse permanent-magnetic nanoparticles with a high degree of desired atomic ordering have been demonstrated by chemical, cluster-deposition and surfactant-assisted ball-milling methods. These studies show that hard magnetic nanoparticles can be combined with an appropriate soft phase to form exchange-coupled nanocomposites to enhance the energy density in nanoparticle-based permanent magnets. However, the easy-axis alignment of the hard phase and self-assembly of these nanocomposites are important processing steps that need to be developed for the enhancement of the remanent magnetization and achievement of high packing densities, respectively. In addition, an efficient exchange-decoupling between the nanocomposite particles proposed in the present study is advantageous to maintain the coercivity of the hard phase and also allow a large inclusion of soft phase typically ~50 vol.% or above. These considerations suggest that appropriate processing steps and nanostructuring of nanoparticle building blocks have the potential to produce future permanent magnets with giant energy products of order 100 MGOe. Several issues including nanoscale processing, scale-up and compaction will require much additional research.

Acknowledgments — This work is supported by Advanced Research Projects Agency-Energy (Grant No. DE-AR 0000046, to B.B. and G.C.H.), Department of Energy (Grant No. DE-FG02–04ER46152, to D.J.S.), NSF – Materials Research Science and Engineering Center (Grant # DMR-0820521, to R.S.) and the Nebraska Center for Materials and Nanoscience.

References

[1] J.M.D. Coey, J. Mag, Mag. Mat. 248 (2002) 441.
[2] K.J. Strnat, Proc. IEEE 78 (1990) 1.
[3] R. Skomski, J.E. Shield, D.J. Sellmyer, Mag. Technol. Int. 1 (2011) 26.
[4] N. Jones, Nature 472 (2011) 22.
[5] E. Kneller, Ferromagnetism, Springer Verlag, Berlin, 1962.
[6] R. Skomski, J.M.D. Coey, Permanent Magnetism, Institute of Physics, Bristol, 1999.
[7] K. Strnat, G. Hoffer, J. Olson, W. Ostertag, J.J. Becker, J. Appl. Phys. 38 (1967) 1001.
[8] R. Skomski, J. Phys.: Condens. Matter. 15 (2003) R841.
[9] S. Sun, C.B. Murray, D. Weller, L. Folks, A. Moser, Science 287 (2000) 1989.
[10] H. Zeng, J. Li, J.P. Liu, Z.L. Wang, S. Sun, Nature 420 (2002) 395.
[11] D.J. Sellmyer, Nature 420 (2002) 374.
[12] D.J. Sellmyer, C.P. Luo, Y. Qiang, J.P. Liu, Magnetism of nanophase composite films, in: H.S. Nalwa (Ed.), Hand Book of Thin Films, Academic Press, New York, 2002, pp. 337–374.

[13] Y. Hou, Z. Xu, S. Peng, C. Rong, J.P. Liu, S. Sun, Adv. Mater. 19 (2007) 3349.

[14] N. Tang, Z. Chen, Y. Zhang, G.C. Hadjipanayis, F. Yang, J. Mag, Mag. Mat. 219 (2000) 173.

[15] D. Alloyeau, C. Ricolleau, C. Mottet, T. Oikawa, C. Langlois, Y. Le Bouar, N. Braidy, A. Loiseau, Nat. Mater. 8 (2009) 940.

[16] E.P. Wohlfarth, J. Appl. Phys. 29 (1958) 595.

[17] J. Li, Z.L. Wang, H. Zeng, S. Sun, J.P. Liu, Appl. Phys. Lett. 82 (2003) 3743.

[18] B. Balasubramanian, R. Skomski, X.Z. Li, S.R. Valloppilly, J.E. Shield, J.E. Shield, G.C. Hadjipanayis, D.J. Sellmyer, Nano Lett. 11 (2011) 1747.

[19] B. Balasubramanian, R. Skomski, X.Z. Li, S.R. Valloppilly, J.E. Shield, J.E. Shield, G.C. Hadjipanayis, D.J. Sellmyer, J. Appl. Phys. 109 (2011) 07A707.

[20] Y.C. Sui, Y. Zhou, X.Z. Li, D.J. Sellmyer, J. Appl. Phys. 99 (2006) 08G704.

[21] Y.C. Sui, W. Liu, L.P. Yue, X.Z. Li, Y. Zhao, R. Skomski, D.J. Sellmyer, J. Appl. Phys. 97 (2005) 10J304.

[22] K. Elkins, D. Li, N. Poudyal, V. Nandwana, Z. Jin, K. Chen, J.P. Liu, J. Phys. D: Appl. Phys. 38 (2005) 2306.

[23] V. Nandwana, K.E. Elkins, N. Poudyal, G.S. Chaubey, K. Yano, J.P. Liu, J. Phys. Chem. C 111 (2007) 4185.

[24] H. Zhang, S. Peng, C. Rong, J.P. Liu, Y. Zhang, M.J. Kramer, S. Sun, J. Mater. Chem. 21 (2011) 16873.

[25] T. Matsushita, T. Iwamoto, M. Inokuchi, N. Toshima, Nanotechnology 21 (2010) 095603.

[26] H. Haberland, M. Karrais, M. Mall, Y. Thurner, J. Vac. Sci. Technol. A 10 (2000) 3266.

[27] B. Balamurugan, R. Skomski, G.C. Hadjipanayis, D.J. Sellmyer, J. Appl. Phys. 111 (2012) 07B527.

[28] O.A. Akdogan, W. Li, G.C. Hadjipanayis, D.J. Sellmyer, J. Nanopart. Res. 13 (2011) 7005.

[29] Y. Xu, M.L. Wan, J. Zhou, D.J. Sellmyer, J. Appl. Phys. 97 (2005) 10J320.

[30] J.M. Qiu, J.P. Wang, Appl. Phys. Lett. 88 (2006) 192505.

[31] D.L. Peng, T. Hihara, K. Sumiyama, Appl. Phys. Lett. 83 (2003) 350.

[32] Y. Xu, M.L. Yan, D.J. Sellmyer, Cluster-assembled nanocomposites, in: D.J. Sellmyer, R. Skomski (Eds.), Advanced Magnetic Nanostructures, Springer Verlag, New York, 2006, pp. 207–238.

[33] A. Terheiden, O. Dimitrieva, M. Acet, C. Mayer, Chem. Phys. Lett. 431 (2006) 113.

[34] A. Terheiden, C. Mayer, K. Moh, B. Stahlmecke, S. Stappert, M. Acet, B. Rellinghausas, Appl. Phys. Lett. 84 (2004) 3891.

[35] N. Poudyal, C. Rong, J.P. Liu, J. Appl. Phys. 107 (2010) 09A703.

[36] Y. Wang, Y. Li, C. Rong, J.P. Liu, Nanotechnology 18 (2007) 465701.

[37] N.G. Akdogan, G.C. Hadjipanayis, D.J. Sellmyer, Nanotechnology 21 (2010) 295705.

[38] N.G. Akdogan, G.C. Hadjipanayis, D.J. Sellmyer, J. Appl. Phys. 105 (2009) 07A710.

[39] N.G. Akdogan, W. Li, G.C. Hadjipanayis, J. Appl. Phys. 109 (2011) 07A759.

[40] J. Zhou, R. Skomski, K.D. Sorge, D.J. Sellmyer, Scripta Mater. 53 (2005) 453.

[41] B. Balamurugan, R. Skomski, D. Le Roy, G.C. Hadjipanayis, J.E. Shield, D.J. Sellmyer, Cluster synthesis, direct ordering, and alignment of rare-earth transition-metal nanomagnets, in: M.D. Salazar-Villalpando, N.R. Neelameggham, D.P. Guillen, S. Pati, K. Krumdick (Eds.), Energy Technology 2012: Carbon Dioxide Management and Other Technologies, TMS (The Minerals, Metals & Materials Society), 2012, pp. 393–398.

[42] J.M. Qiu, J. Bai, J.P. Wang, Appl. Phys. Lett. 89 (2006) 222506.

[43] X. Liu, S. He, J.M. Qiu, J.P. Wang, Appl. Phys. Lett. 98 (2011) 222507.

[44] S. Kang, Z. Jia, S. Shi, D.E. Nikles, J.W. Harrell, Appl. Phys. Lett. 86 (2003) 062503.

[45] S. Kang, S. Shi, Z. Jia, G.B. Thomson, D.E. Nikles, J.W. Harrell, D. Li, N. Poudyal, V. Nandwana, J.P. Liu, J. Appl. Phys. 101 (2007) 09J113.

[46] J.W. Harrell, S. Kang, S. Shi, Z. Jia, D.E. Nikles, R. Chantrell, A. Satoh, Appl. Phys. Lett. 87 (2005) 202508.

[47] Y. Zhang, M.J. Kramer, C. Rong, J.P. Liu, Appl. Phys. Lett. 97 (2010) 032506.

[48] C. Rong, Y. Zhang, N. Poudyal, X. Xiong, M.J. Kramer, J.P. Liu, Appl. Phys. Lett. 96 (2010) 102513.

[49] Z.M. Chen, X. Meng-Burany, H. Okumura, G.C. Hadjipanayis, J. Appl. Phys. 87 (2000) 3409–3414.

[50] R. Coehoorn, D.B. de Mooij, C. de Waard, J. Magn. Magn. Mat. 80 (1989) 101.

[51] E.F. Kneller, R. Hawig, IEEE Trans. Magn. 27 (1991) 3588.

[52] R. Skomski, J.M.D. Coey, Phys. Rev. B 48 (1993) 15812.

[53] J.P. Liu, Exchange-coupled nanocomposite permanent magnets, in: J.P. Liu, E. Fullerton, O. Gutfleisch, D.J. Sellmyer (Eds.), Nanoscale Magnetic Materials and Applications, Springer Verlag, New York, 2009, pp. 309–335.

[54] X. Rui, J.E. Shield, Z. Sun, Y. Xu, D.J. Sellmyer, Appl. Phys. Lett. 89 (2006) 122509.

[55] X. Rui, J.E. Shield, Z. Sun, R. Skomski, Y. Xu, D.J. Sellmyer, M.J. Kramer, Y.Q. Wu, J. Mag, Mag. Mater. 320 (2008) 2576.

[56] Y. Liu, T.A. George, R. Skomski, D.J. Sellmyer, Appl. Phys. Lett. 99 (2011) 172504.

[57] B. Balasubramanian, K.L. Kraemer, N.A. Reding, R. Skomski, S. Ducharme, D.J. Sellmyer, ACS Nano 4 (2010) 1893.

[58] B. Balasubramanian, K.L. Kraemer, S.R. Valloppilly, S. Ducharme, D.J. Sellmyer, Nanotechnology 22 (2011) 405605.

[59] J.P. Wang, J. Bai, Appl. Phys. Lett. 87 (2005) 152502.